The International Journal of Advanced Manufacturing Technology (2024) 131:5787–5799
https://doi.org/10.1007/s00170-024-13298-0

ORIGINAL ARTICLE

Flexible actuation with intrinsic sensing for ram extrusion 3D printing

Setthibhak Suthithanakom[1] · Chaiwuth Sithiwichankit[1] · Kantawatchr Chaiprabha[1,2] · Ratchatin Chancharoen[1,2]

Received: 27 October 2023 / Accepted: 18 February 2024 / Published online: 4 March 2024

Abstract
Conventional actuation mechanisms used in liquid deposition modeling (LDM) technology limit the flow handling capability and the visibility of the printing materials' properties. This work presents a flexible actuation system with intrinsic sensing for a ram extrusion printhead used in LDM technology. A mathematical model is used to design and simulate the printhead. The experimental results demonstrate the system's ability to control the extrusion flow in two modes. The pressure control mode is favorable for the flow in a transient state such as flushing. The volumetric control mode provides a constant printed line width with less than 0.1-mm deviation between each tested material (biogel, chocolate fudge, and silicone sealant). A lower standard deviation for printed lines in the volumetric control mode indicates more precise line printing. The system also incorporates real-time monitoring of extrusion pressure and flow rate. The intrinsic capability to detect printing material properties is validated in both simulation and experiment. It provides valuable insights for further optimization of the printing process. The proposed system offers the advantage of improved pressure and flow control as well as the ability to monitor and respond to the properties of printing material.

Keywords Liquid deposition modeling · Ram extrusion · Actuation and sensing · Viscoelastic material

1 Introduction

Liquid deposition modeling (LDM), also known as direct ink wiring, is an advanced form of 3D printing that utilizes liquid or gel-like materials as the primary medium for creating three-dimensional objects [1, 2]. This fabrication process features most of the benefits of additive manufacturing. Furthermore, it supports a wide range of materials, including polymers [3, 4], ceramics [5, 6], metals [7, 8], and even biological materials like hydrogels [9, 10]. This versatility makes it applicable across various industries, each with unique material requirements [1]. Recently, studies on the extrusion printing of nanomaterials, utilizing their astonishing properties, are also investigated [11, 12].

Studies on the evaluation process for the potential new printing materials have been also carried out [13, 14]. A notable example is the printing of biomaterials [15]. Great precision is required for the deposition of living cells and biomaterials to create functional tissue structures for transplantation or research purposes [10, 16]. Much research has been carried out to develop a reliable and precise fabrication process. The scope of this work incorporates (a) biomaterial for functional tissues and organs [2, 9], (b) material extrusion that precisely controls the flow of material including in situ parameters [17], (c) curing and solidification [18], and (d) post-processing [19].

As regards advanced 3D printing of biomaterials toward various tissues and organs, it is found that biomaterials must mimic complex living tissues while their properties are also expected to favor the 3D printing processes [20].

Chaiwuth Sithiwichankit, Kantawatchr Chaiprabha, and Ratchatin Chancharoen contributed equally to this work.

✉ Ratchatin Chancharoen
ratchatin.c@chula.ac.th

Setthibhak Suthithanakom
setthibhak@gmail.com

Chaiwuth Sithiwichankit
chaiwuth.cs@gmail.com

Kantawatchr Chaiprabha
kant.chai@gmail.com

[1] Department of Mechanical Engineering, Chulalongkorn University, 254 Phaya Thai Road, Bangkok 10330, Thailand

[2] Human-Robot Collaboration and Systems Integration Research Unit, Chulalongkorn University, 254 Phaya Thai Road, Bangkok 10330, Thailand

Most biomaterials physically express viscoelastic behavior, exhibiting the complex characteristics of both elastic solid and viscous fluid [2].

To achieve the desired structure of the biomaterials, it must be deposited with high accuracy. For this purpose, extrusion flow must be precisely controlled. However, the mechanical properties of biomaterials tend to be unknown a priori and vary during the 3D printing process. There are three common approaches for extrusion gel-like materials: pneumatic actuation, piston actuation, and screw actuation (Fig. 1). The pneumatic actuation method relies on the fundamentals of controlling the printing pressure through compressed air. This procedure provides reliable extrusion flow only if biomaterials have few variations in mechanical properties. To handle such materials with greater variation, piston actuation has been employed together with motion control. The common method of piston actuation is via a lead screw or ball screw using a stepper motor [21]. When rotation motion is applied, the piston is pushed down and the material is extruded. This allows the flow to be reliably obtained in a steady state. Similarly, screw actuation performs by precisely controlling the flow, utilizing the rotation of the screw. It is seen that screw actuation gains benefit over the piston by allowing the extrusion of highly viscous material [7].

Despite the success in flow control for these two positive displacement actuations, i.e., piston and screw actuation, extrusion flow in a transient state cannot be controlled deterministically. The viscoelasticity of biomaterials plays a key role in this challenge. Due to the elastic behavior of the material, pressure manipulation is required to gain control over the flow. Further studies are required to overcome this problem.

Herein, this research presents the development of a novel piston-driven material extruder having the features of flexible actuation and intrinsic sensing. Flexible actuation refers to the concept of controlling either the extrusion pressure or volumetric flow, one at a time. Each mode is suitable for transient and steady-state flow of the viscoelastic materials, respectively. The ability to shuffle between two modes on the fly proposes better control over the printing process, compared to single-mode operation [22].

Intrinsic sensing is the perception of the mechanical properties of biomaterials during extrusion along with pressure and flow rate, which are critical parameters for the printing process. This type of actuation highlights the possibility of control over the extrusion of materials that are not specifically tuned for 3D printing [23].

In this paper, mathematical analysis, simulation, and experiments have been used to demonstrate the benefits of the proposed design. As such, work on flexible actuation providing control over the whole extrusion process, with pressure controlled for transient state handling and volumetric controlled for precise extrusion at steady state, has been limited. Our work sets out to expand upon previous research. It is noted that intrinsic sensing not only is the foundation of flexible actuation but also enhances the performance of this design. By enabling real-time sensing of material properties, many useful features can be developed and implemented in the process, e.g., on-the-fly detection of anomalies such as clogging, bubbles, and sediment.

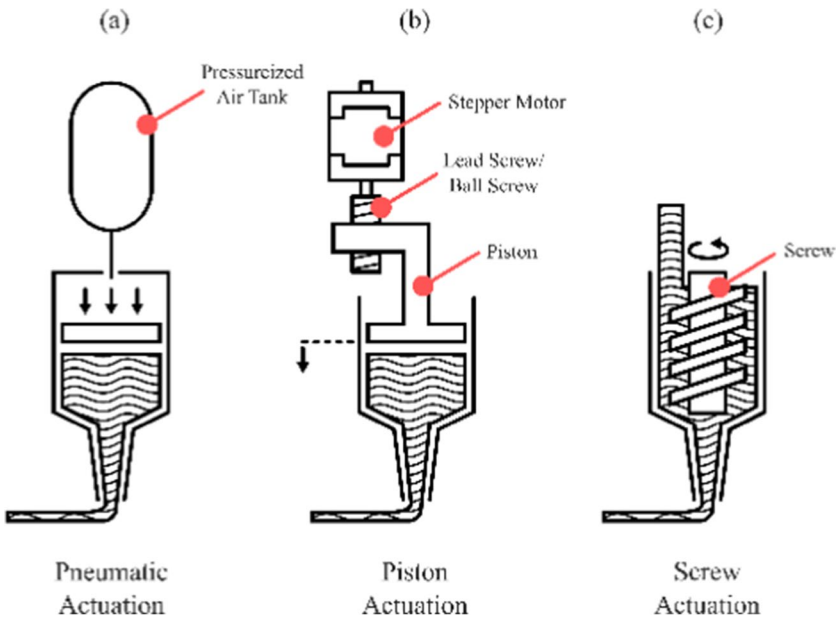

Fig. 1 Types of actuation technique: **a** pneumatic actuation utilizes the pressurized air in the tank to push the material, **b** piston actuation, the stepper motor and lead screw/ball screw are used to displace the piston, and **c** screw actuation uses a rotating screw to directly displace the material

2 Methodology

2.1 Modeling ram extruder

The proposed ram extrusion was designed to effectively control the flow of printing material via two modes: either by (1) pressure or (2) volumetric flow control. When the ram extruder is under pressure control, the volumetric flow rate can be monitored. Vice versa, if the ram extruder is in volumetric flow control, the pressure inside the syringe can be monitored. The actuator, for the ram extrusion, is commanded by a control signal and can provide sufficient force to extrude the material out of the syringe. In this case, a permanent magnet DC motor is preferred, compared to a stepper motor. As a result, the motor model is less complex, and the flexible control mode can be implemented, as described in this section.

The voltage of a DC motor can be determined using the following equation, indicating that the current is dependent on both the voltage and the rotational speed of the motor:

$$V = L_m\dot{I} + K_V\omega + R_m I \tag{1}$$

where V denotes the voltage; I denotes the electrical current, which flows through an armature coil; and ω represents the motor speed.

In the modeling of the ram extruder, the following parameters and variables are used, as shown in Tables 1 and 2.

The resulting torque of the permanent magnet DC motor is proportional to the current I that flows through the motor coil. The torque T generated by the motor can be derived from the motor's electrical current I as:

$$T = K_T I \tag{2}$$

Table 1 Parameters

Symbols	Values	Unit	Description
R_m	4	Ω	Motor resistance
L_m	99.5	μH	Motor inductance
K_V	0.0261	V·s/rad	Motor velocity constant
K_T	0.0261	N·m/A	Motor torque constant
J	0.001	kg·m^2	System moment of inertia
f	30	N	System friction
r	0.001	m	Screw radius
α	4.55	deg	Lead angle
μ	0.05	N/A	Screw friction coefficient
D	0.0148	m	Syringe inner diameter
M	0.08	kg	Carriage mass
m	N/A	kg	Material mass
k	N/A	N/m	Material spring constant
c	N/A	N·s/m	Material damping coefficient

Table 2 Variables

Symbols	Unit	Description
X_1	m	Displacement of piston
X_2	m	Displacement of material entering nozzle
θ	rad	Angular displacement of screw
ω	rad/s	Angular velocity of screw
V	V	Voltage
I	A	Current
T	N·m	Motor torque
F	N	Screw load
P	Pa	Syringe pressure
Q	m^3/s	Volumetric flow rate

If the applied voltage V is commanded and the motor speed ω is monitored in real-time, the output torque T can be approximated by the mathematical model, as described in Eqs. (1) and (2).

The motor is designed to run at high speed but only provides a small output torque. Transmission is required to provide mechanical advantages such that the speed is lowered and output torque is increased having the same power rating. In this case, a mechanism to convert the rotational motion of the motor into linear motion that can drive the piston is needed. It is noted that syringes are cylindrical and their pistons move in pure translation. For the proposed design, a ball screw was selected since it can provide mechanical advantages and can convert rotational motion into linear motion. To connect the output shaft of the motor to the ball screw, a flexible coupling is used. The coupling frees other axes except the rotational axis where both shafts are interfaced. In this design, the ball screw ensures rigid transmission between the shaft of the motor and the linear motion of the piston. The feed position of the piston x_1 can be derived by the kinematic relationship of the ball screw [24]:

$$x_1 = r\ \tan(\alpha)\theta \tag{3}$$

Although the screw enables a favorable over-motion conversion and mechanical advantage, it exhibits unavoidable friction between the relative surfaces of the nut and screw. Such friction has asymmetric properties, is hard nonlinear, time-variant, and sensitive to disturbance. The point at which friction occurs is between the rotational and translational domains; thus, the complication is amplified.

The coulomb friction model is used for representing the friction in a screw. The angle of friction γ can be written in the form of the coulomb coefficient μ as:

$$\gamma = \begin{cases} -\tan^{-1}(\mu); \textit{backward drive} \\ \tan^{-1}(\mu); \textit{forward drive} \end{cases} \tag{4}$$

It is acknowledged that γ can be varied by following the driving direction of the mechanism. Hence, the equation of motion of the carriage can be defined as:

$$\left(Mr\ tan(a+\gamma)+\frac{1}{rtan(a)}\right)\ddot{x}_1 = T - Fr\ tan(a+\gamma) \tag{5}$$

If the motion of the system is determined by the effort from the rotation of the screw, the direction is called forward drive. Vice versa, if the effort from the nut drives the system, the direction is backward. Mechanical advantage varies depending on the driving direction, whereas backward driving delivers more mechanical advantage. The reason behind this effect lies in the interaction of the screw's nonlinear behavior and the friction. By operating in a backward drive, the negative value of γ reduces the value of $(\alpha+\gamma)$ inside the tangent function. This reduction reduces the influence of load F, generating a higher mechanical advantage. As for a screw with a small lead angle α, the effect of negative γ is large enough such that $(\alpha+\gamma)$ is zero or negative. This outcome prevents the effect of the action on the nut side to the system, which is called non-back drivable. The screw that possesses this behavior has self-locking ability.

Loaded material is typically viscoelastic such that its behavior is a blend between viscous fluid and elastic solid. To precisely control the flow of such material, two material properties are implemented. The first one is elastic modulus, which explains the elastic response of the material. The second one is viscosity, which describes the resistance of a fluid to flow. The fluid aspect of viscoelastic material that is mostly used in LDM is a non-Newtonian fluid; the relationship between shear rate and shear stress is nonlinear [2]. Thus, the nonlinear resistance of the flow is exhibited.

As for the aspect of modeling, the lumped element model is used to describe the material. Elasticity is represented by a spring whose spring constant k corresponds to the elastic modulus of the material. The viscous element can be modeled as a damper with a nonlinear damping coefficient $c(\dot{x_2})$, corresponding to the viscosity, where x_2 is a displacement of material that enters the nozzle. It is assumed that the elastic behavior is dominated only in the syringe, while the viscous effect is mainly presented in the nozzle. A small amount of extruded mass is neglected. The spring is connected to the damper in series; a mass of the material that is inside the nozzle m is attached between them.

Let the displacement of material that is entering the nozzle be x_2. The load that acts as a piston can be defined by the spring effect inside the syringe as:

$$F = f + k(x_1 - x_2) \tag{6}$$

where f is the overall friction, which resists the system's motion. The equation of motion can then be derived as follows:

$$m\ddot{x}_2 = \mathrm{k}\left(x_1 - x_2\right) - \mathrm{c}(\dot{x_2})\dot{x_2} \tag{7}$$

where $c(\dot{x_2})$ is a nonlinear damping coefficient:

$$c(\dot{x_2}) = c_1 + c_2\ sgn\ (\dot{x_2})\dot{x_2} \tag{8}$$

When all the governing Eqs. (1)–(8) have been presented, a stability analysis of the system is carried out. Lyapunov's second method can be used to guarantee the stability of nonlinear dynamical systems. Subsequently, the Lyapunov candidate function $\Upsilon(X)$, as represented by the summation of the kinetic energy of the screw and material, electrical energy in the motor, plus the energy from viscoelastic material deformation, yields [25]:

$$\Upsilon(X) = \frac{k\left(x_1 - x_2\right)^2}{2} + \frac{L_m I^2}{2} + \frac{m_t \dot{x_1}^2}{2} + \frac{m\dot{x_2}^2}{2} \tag{9}$$

Such a function is in a quadratic form, holding the condition at stable point: $\Upsilon(0) = 0$, and the positive definition becomes $\Upsilon(X) = 0$ if $X \neq 0$.

The derivative form of the candidate function is derived as follows:

$$\dot{\Upsilon}(X) = J_t \ddot{x_1}\dot{x_1} + k\left(\dot{x_1} - \dot{x_2}\right)\left(x_1 - x_2\right) + m\ddot{x_2}\dot{x_2} + L_m I\dot{I} \tag{10}$$

Substituting Eqs. (1)–(7) in the derivative form of the candidate function and voltage $V=0$ results in:

$$\dot{\Upsilon}(X) = -R_m I^2 - c(\dot{x_2})\dot{x_2}^2 - f\dot{x_1} - \left(\frac{K I\dot{x_1}}{r\ tan(\alpha)} - \frac{K I\dot{x_1}}{r\ tan(\alpha+\gamma)}\right) \tag{11}$$

To prove Lyapunov's stability [25], the state must converge at a stable point so that $\dot{\Upsilon}(X) < 0$. It is noted that in the case of asymptotic stability, such conditions must hold true for $X \neq 0$.

The first term $R_m I^2$ is a power loss by the resistance of the motor, which is always positive. The second term $c(\dot{x_2})\dot{x_2}^2$ is a loss in the nonlinear damper:

$$c(\dot{x_2})\dot{x_2}^2 = (c_1 + c_2\ sgn\ (\dot{x_2})\dot{x_2})\dot{x_2}^2 \tag{12}$$

By expanding $sgn(\dot{x_2})$, the term can be written as:

$$c(\dot{x_2})\dot{x_2}^2 = c_1\dot{x_2}^2 + c_2\frac{\dot{x_2}^4}{|\dot{x_2}|} \tag{13}$$

and proves to be positive at $\dot{x_2} \neq 0$.

When considering friction loss $f\dot{x_1}$, the direction of friction always resists the motion of x_1. Thereby, coulomb viscous friction occurs and is defined as:

$$f = sgn\left(\dot{x_1}\right)|f| = \frac{\dot{x_1}}{|\dot{x_1}|}|f| \tag{14}$$

Consequently, $f\dot{x_1}$ can be written as:

$$f\dot{x_1} = \frac{\dot{x_1}^2}{|\dot{x_1}|}|f| \tag{15}$$

This term is always positive. The fourth and fifth terms of Eq. (11) can be expressed as follows:

$$\frac{K I\dot{x_1}}{r\,tan\,(\alpha)} - \frac{K\,I\,\dot{x_1}}{r\,tan\,(\alpha+\gamma)} = \frac{K I\dot{x_1}}{r} \cdot \left(\frac{tan\,(\alpha+\gamma) - tan\,(\alpha)}{tan\,(\alpha)\,tan\,(\alpha+\gamma)}\right) \tag{16}$$

According to the direction of the driving, i.e., forward and backward drive, it is seen that the friction angle γ varies. Direction can be assumed to be dependent on the energy flow of the screw. The power of the motor $K I\dot{x_1}$ can be an indicator of the driving direction. If $K I\dot{x_1}$ is positive, the motor gives power to the system, and the screw is in forward drive. Thus, the friction angle can be written case-wise:

$$\gamma = \begin{cases} -\gamma_{abs}; K I\dot{x_1} < 0 \\ \gamma_{abs}; K I\dot{x_1} > 0 \end{cases} \tag{17}$$

In the case of $K I\dot{x_1} < 0$

$$\left(\frac{tan\left(\alpha - \gamma_{abs}\right) - tan(\alpha)}{tan(\alpha)tan\left(\alpha - \gamma_{abs}\right)}\right) < 0 \tag{18}$$

and when $K I\dot{x_1} > 0$,

$$\left(\frac{tan\left(\alpha + \gamma_{abs}\right) - tan(\alpha)}{tan(\alpha)tan\left(\alpha + \gamma_{abs}\right)}\right) > 0 \tag{19}$$

In these two cases, the sum of the two terms is always positive:

$$\frac{K I\dot{x_1}}{r\,tan(\alpha)} - \frac{K\,I\,\dot{x_1}}{r\,tan(\alpha+\gamma)} > 0 \tag{20}$$

Overall, the four terms regarding the derivative of the Lyapunov candidate function are always negative. Therefore, at any initial state X, the system tends toward stability. Thus, the energy that is stored in the system is always reduced.

After the stability of the system is discussed, the ability to sense and control both the pressure and volumetric flow rate of the material is presented. When in motion, both pressure P and volumetric flow rate Q are visible on the actuator's side. Yet, when the motor and the piston stop, and flow ceases, the friction is in static friction. Friction behavior falls in the dead-band, and the pressure P is invisible on the actuator's side.

The force pushing the material through the nozzle is analogous to the force exerted by the spring which is equal to $F - f$. The pressure of the material at the nozzle entrance P can be estimated as:

$$P = \frac{4(F-f)}{\pi D^2} \tag{21}$$

Equations (1)–(5) show that the force at the piston F can be calculated by the controllable voltage V and the measured motor's position θ. The force can then be used in Eqs. (6) and (21) to obtain the volumetric flow rate Q (directly proportional to x_2) and pressure P, respectively. This proves that by measuring and controlling only two variables: the applied voltage V and the motor's position θ, both the pressure P and volumetric flow rate Q of the system can be derived and manipulated at any given time. However, since both are directly affected by the same variables, only one of them can be controlled at a time:

$$P = \frac{4\left(\frac{K_T\,(V - K_V\omega)}{R_m} - f\,r\tan(\alpha+\gamma)\right)}{D^2\,r\,\pi\tan(\alpha+\gamma)} \tag{22}$$

Furthermore, at steady state, the elastic behavior of the material is disregarded, meaning that the rate of change for x_1 and x_2 are coupled. Thus, the volumetric flow rate Q of the material can then be derived from the motor's speed ω via Eq. (3). By applying the closed-loop controller over the measured motor's position θ, the steady-state volumetric flow rate Q can be directly handled. Similarly, at steady state, only the voltage is required to control the pressure. It is important to note that the pressure inside the nozzle is the gradient from the pressure P to the atmospheric pressure:

$$Q = \frac{\pi\,D^2\,\dot{x_2}}{4} \tag{23}$$

By rearranging all the equations, only the motor's speed ω is required to approximate the volumetric flow rate Q at steady state, as follows:

$$Q = \frac{\pi\,D^2\,r\,tan(\alpha)\,\omega}{4} \tag{24}$$

Subsequently, the pressure P and the volumetric flow rate Q at steady state is thus determined via (1) the applied voltage V, (2) the time derivative of the motor's position θ, and (3) the model.

It is noted that if both the pressure P and the volumetric flow rate Q are controlled, the printing process is enhanced [22]. The technique of flexible actuation is an excellent candidate to control the flow of the material.

2.2 Material properties sensing

Apart from the pressure P and the volumetric flow Q, the intrinsic sensing feature allows the extruder to sense the properties of material. In this simulation, the detection of

the viscosity of the material $c(\dot{x}_2)$ is demonstrated. At steady state, combining Eqs. (1)–(7), $c(\dot{x}_2)$ can be determined:

$$c(\dot{x}_2) = \frac{\left(V_t - K_V\omega(t)\right)\frac{K_T}{R_m} - fr\tan(\alpha+\gamma)}{r^2\tan(\alpha+\gamma)\tan(\alpha)\omega(t)} \tag{25}$$

At steady state, where the applied voltage V is controlled, the motor's speed ω is calculated via the measured motor's position θ. All intrinsic parameters are a *priori* known. Equation (25) demonstrates the proposed model's ability to sense the damping coefficient c of the damper used in the model. The damper represents the viscosity of the material. The proposed ram extruder was simulated via the MATLAB Simscape model (Fig. 2c). The model was constructed through a bond graph approach, where each element is interfaced with both effort and flow signals [26]. In Table 1, the parameters of the simulation can be found.

To validate the prediction of the viscosity, the applied voltage V was applied at various levels of 8, 10, and 12 V. Materials whose damping coefficients were unknown to the system were tested. The damping coefficient of these materials spanned the range of 0 to 10,000 N·s/m with 1000 N·s/m increments.

The motor's speed ω is obtained to predict the damping coefficient of the loaded material via Eq. 10. In the case where the parameter in the system is imprecisely modeled, a simulation is used to demonstrate that the technique is still effective. In the simulation, the friction is assumed to be imprecisely modeled with ± 5% error. Hence, the deviation, resulting from an error in the friction input, is proportionally

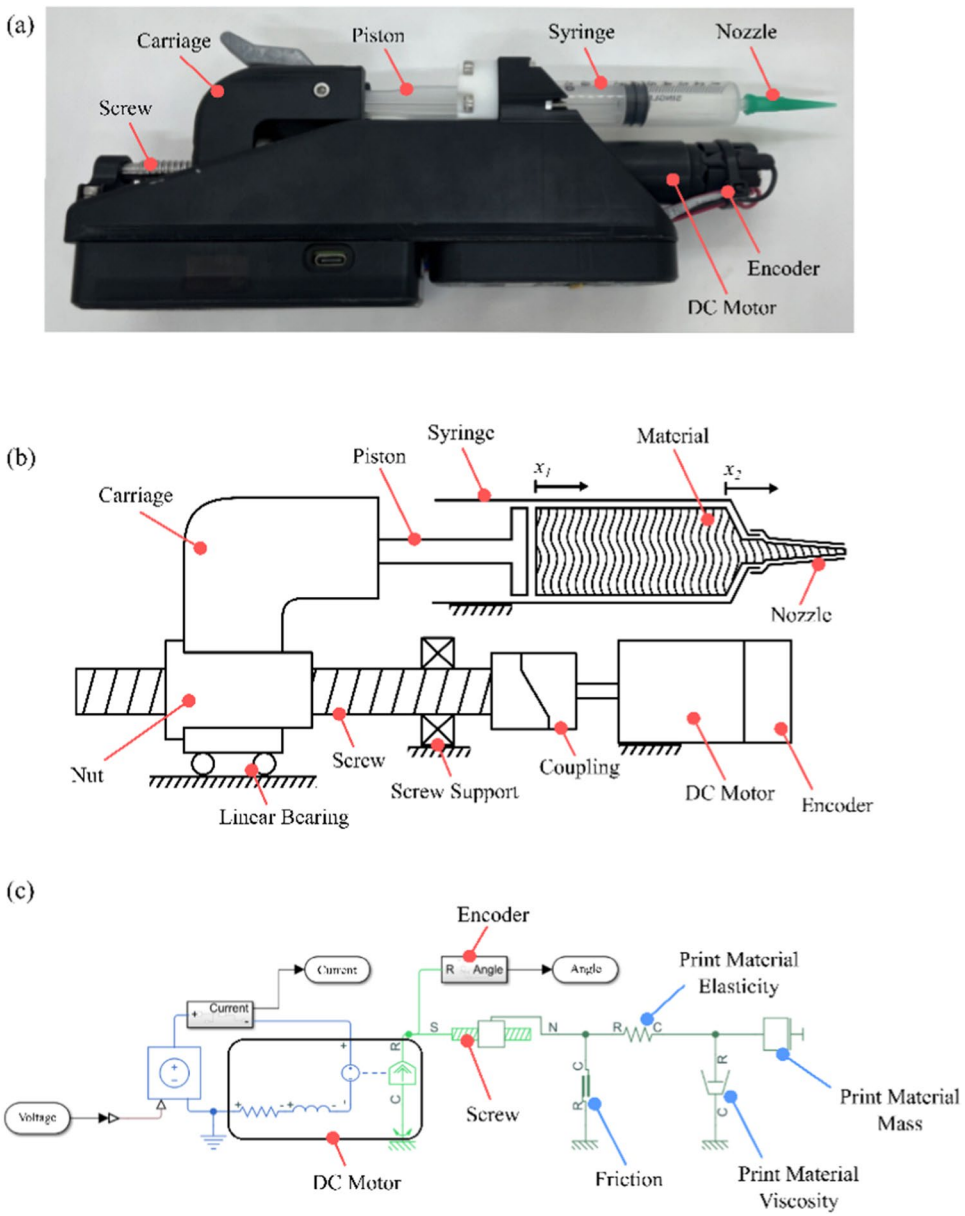

Fig. 2 Ram extruder with flexible actuation and intrinsic sensing for 3D printing: **a** fabricated hardware, **b** schematics, and **c** bond graph diagram

constant for different values of the damping coefficient. Accordingly, + 5% friction error results in guesses higher than the input values and vice versa for − 5% (Fig. 3). The higher voltage suggests lower deviations and greater immunity to the change in hardware parameters.

2.3 Hardware description

A custom extruder printhead was designed and fabricated based on the proposed concept (Fig. 2a). A Faulhaber DC motor 2342S024CR with magnetic encoder IE3-1024 L was selected as the actuator. It was connected to THK ball screw BNK0802 via a flexible coupling. The chassis and other passive components of the extruder were 3D printed, using photocurable resin. The chassis is designed so that a 10-mL syringe main body can be clamped onto it, while the syringe piston movement is coupled with the ball screw nut.

To control the extruder hardware, a custom-designed PCB was used. This PCB utilizes a DRV8876PWPR DC motor driver chip, which features the current sensing ability, allowing real-time measurement of the electrical current supplied to the motor. To handle both communication and signal processing, the STM32-based microcontroller was employed. Its firmware was specially designed to switch between constant voltage mode (pressure controlled) and closed-loop mode (volumetric controlled). In the closed-loop mode, a proportional derivative controller was applied to precisely manipulate the movement of the motor. Both position and the electrical current of the motor were signified by the microcontroller and were logged over time for usage in the experiments. The size of the assembly without the syringe is roughly 220 × 110 × 50 mm, and its weight is 622 g. The maximum power is 24 W. This system gives the maximum pressure exceeding 7 Bars and maximum volumetric flow of approximately 6 mL/s at no load.

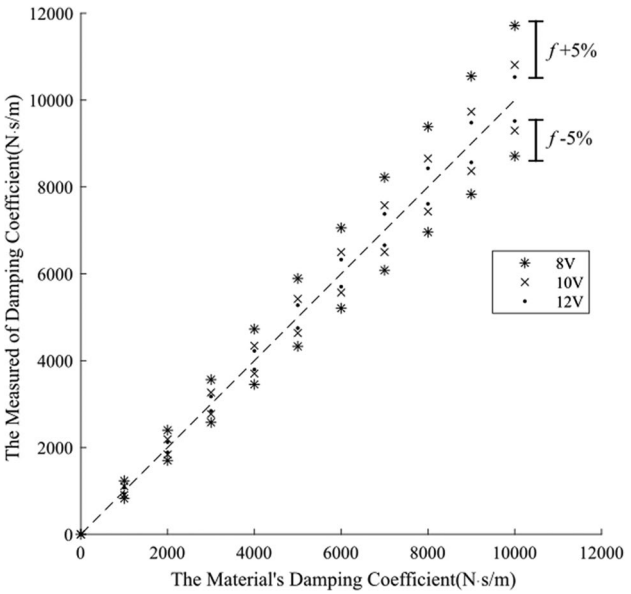

Fig. 3 The simulated results of the damping coefficient measurements are illustrated. The dotted diagonal line represents the correct estimation. Data above this line reveal the results of the input friction error of + 5%. Data below this line represent the friction error of − 5%

Herein, this ram extruder was designed to connect and communicate with consumer 3D printers through a specially designed adapter. The adapter is able to transmit the STEP/DIR/EN signal normally used for stepper-based extruders in typical fused deposition modeling (FDM) printers. In the closed-loop extrusion, the custom extruder receives these signals from the printer and controls the extrusion at the rate of the STEP signal. In addition, the adapter relays the serial communication for the extruder, allowing the usage of the special G-code commands, plus the recordings of the extruder data, including piston position and electrical current.

2.4 Experimental setup

2.4.1 Print materials

To demonstrate the proposed flexible extrusion profiles and intrinsic sensing of the ram extruder, three materials, (a) biogel (5% food-grade gelatin solution), (b) chocolate fudge, and (c) silicone sealant, were chosen. These materials are viscoelastic material that can be 3D printed using the LDM technique. Each material represents different fields, wherein LDM technology provides useful applications, including (a) tissue engineering, (b) food, and (c) engineering, respectively. These materials exhibit different flow behaviors, illustrating how the proposed system will perform using various materials in real-world applications with distinct rheological properties.

2.4.2 Flexible actuation

In this section, experiments were designed to demonstrate the different outcomes between the pressure-controlled and volumetric-controlled modes. During flushing and printing operations, the behavior of the print material was analyzed and compared.

The flushing process of chocolate fudge was performed six times. In the first half of the experiment, different controlled feed rates of 1, 2, and 3 mm/s were executed. In the second half, motor voltages of 8, 10, and 12 V were implemented for constant pressure. Subsequently, to equalize the amount of material extruded for each attempt, extrusion was halted when the piston position reached 3 mm from the starting point. The motor's position θ and the motor's electrical current I were measured, over time.

All three materials mentioned above were used to lay lines 30 mm in length. For each material, four lines were printed. Firstly, using volumetric feed rate of 4.17 mm^3/s, this feed rate provided the cross-sectional area of the line at 0.5 mm^2. Secondly, the remaining lines were printed using pressure-controlled extrusion mode at motor voltages: 6, 8, and 10 V. All the lines were laid at a nozzle height of 0.5 mm and horizontal feed rate of 8.33 mm/s. As such, this study focused on steady-state line properties. Thus, the 60-mm-long square-wave-shaped line was printed immediately before the experimental lines. Thereafter, the images of the lines printed on the glass slides were captured through a telecentric lens. In Fig. 4, the extraction process of both mean and standard deviation of the line widths are shown. Image analysis was used to determine the quality of the printed line.

2.4.3 Intrinsic sensing

Apart from utilizing flexible actuation, the sensed pressure P and volumetric flow rate Q can be used to discern the properties of the print materials. The ability to perceive real-time properties of the print material was validated through a heterogeneous mixture extrusion test. As shown in Fig. 5, the syringe containing the mixture was prepared. The volumetric-controlled extrusion was executed on this non-homogeneous mixture at the reference piston feed rate of 1 mm/s. The piston feed rate was logged over time together with the motor's electrical current I which can be used to validate motor torque T.

3 Results and discussion

3.1 Flexible actuation: flushing process

In Fig. 6, both the measured current I and piston feed rate, from the pressure-controlled and volumetric-controlled flushing of chocolate fudge, are shown. Piston feed rate was calculated via the differentiation of the measured position of the piston, over time. The motor current I represents the torque T generated from the motor, corresponding with the pressure P at steady state.

In the pressure-controlled flushing process, the constant voltage V applied to the motor and the piston initialized the flow of the print material from its resting state. This event resulted in the surge of the motor's electrical current I to certain values. The current I is seen to stabilize around the values up to the end of the process. Hence,

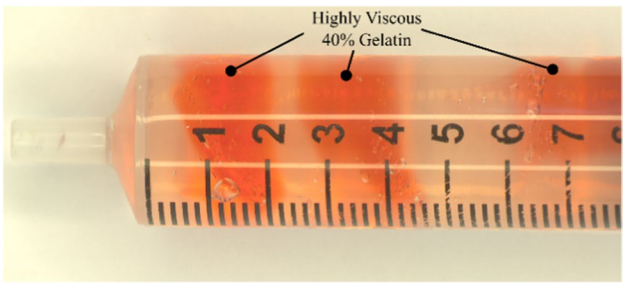

Fig. 5 The heterogeneous mixture of 40% food-grade gelatin in water solution (red) deposited in its 5% counterpart (clear). The mixture is stored in the syringe

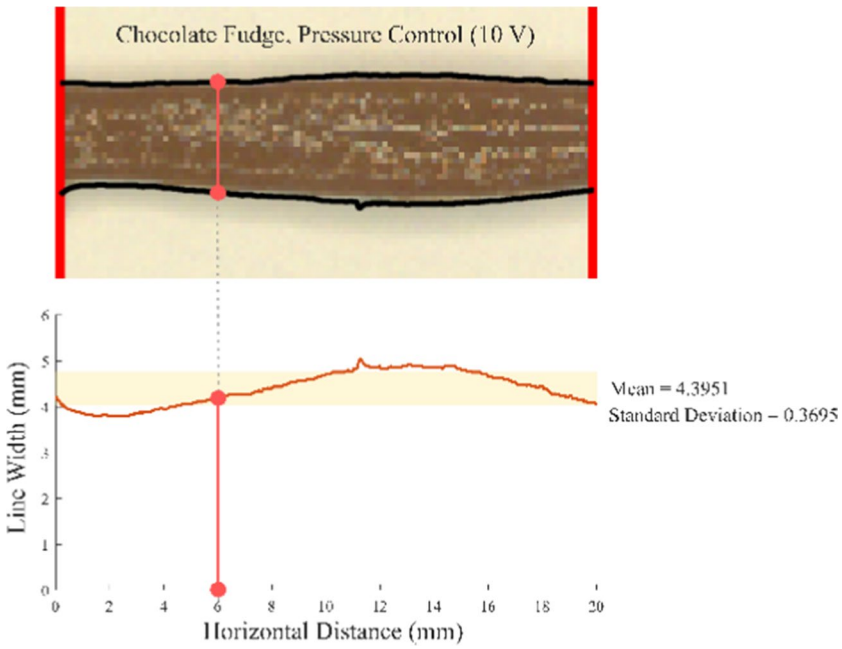

Fig. 4 Line width extraction process. The images of the lines are processed using a binary thresholding technique to find the upper and lower bounds of the lines. Then, the number of pixels between the upper and lower bound at the same vertical position are counted. These numbers are obtained along the selected portion of the printed lines. Subsequently, the mean and standard deviation of the numbers are calculated

it is implied that torque T stabilized around a certain value, depending on the applied voltage V. The elasticity of the material caused the piston feed rate to experience a high magnitude of fluctuation at first, then the feed rate gradually slowed down at a different rate, depending on the applied voltage V.

In the volumetric-controlled flushing process, the motor current I displayed a relatively slower rise. However, due to the complex behavior of the elasticity of the material plus the viscosity, the electrical current fluctuated greatly. In the 3-mm extrusion time frame, the current from each feed rate did not appear to converge to any certain value. After slight instability, the feed rate of the piston continued to stabilize around the controlled reference value.

3.2 Flexible actuation: line printing

The three materials used for printing exhibited different flow behavior and magnitude of deformation resistance. It is seen that silicone sealant displayed the highest viscosity followed by chocolate fudge, and biogel, respectively. In Fig. 7, the images of the printing results of these materials under both extrusion modes are displayed. In Table 3, the mean line width and standard deviation of line width were extracted from each printed line and are outlined.

For each particular material, the mean line width revealed a positive correlation with the motor voltage V. Regarding the viscosity of the materials, the magnitude and the rate of change were diverse. For each particular voltage, silicone sealant was found to have the minimum mean line width followed by chocolate fudge, and biogel. The difference between the smallest and greatest value found was in the order of millimeters. In the volumetric-controlled printing, the difference spanned in the order of hundreds of microns.

As for standard deviation, a positive correlation with voltage was observed, though the correlation displayed worse linearity than that of the mean line width. At each voltage V, the standard deviation also displayed similarity to the mean. Herein, silicone sealant had the lowest deviation, demonstrating the domination of viscosity over elasticity. The highest deviation proved to be in biogel where its superior elasticity caused wobbling in the printed line. Similarly, this trend occurred in the volumetric-controlled printing. When printed in the volumetric-controlled mode, it is important to note that, for each material, the smallest standard deviation was encountered.

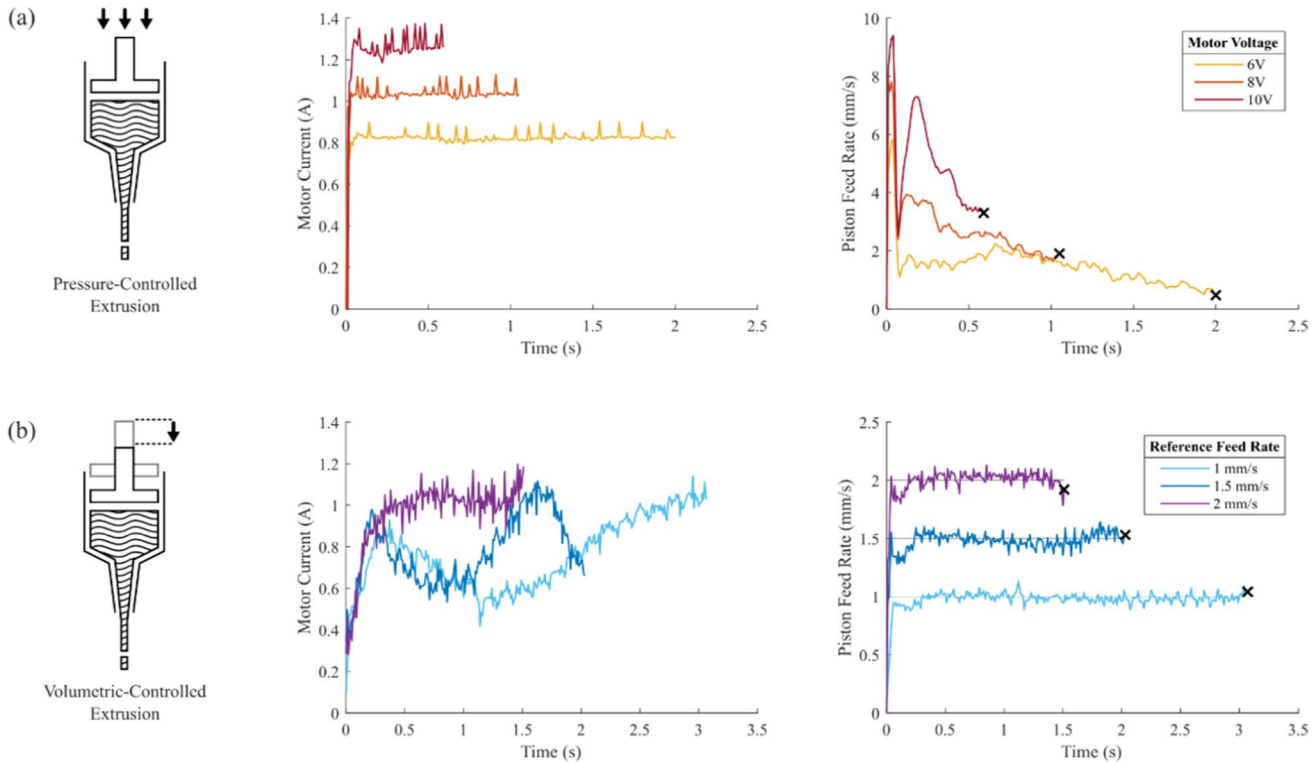

Fig. 6 Experimental data obtained from the flushing operation of the different modes. Pressure-controlled extrusion (**a**) is actuated by 8, 10, and 12 V. Volumetric-controlled extrusion (**b**) is commanded at the piston's reference feed rate of 1, 2, and 3 mm/s. Extrusion ends when a piston displacement of 3 mm is reached, as signified by the black "X"

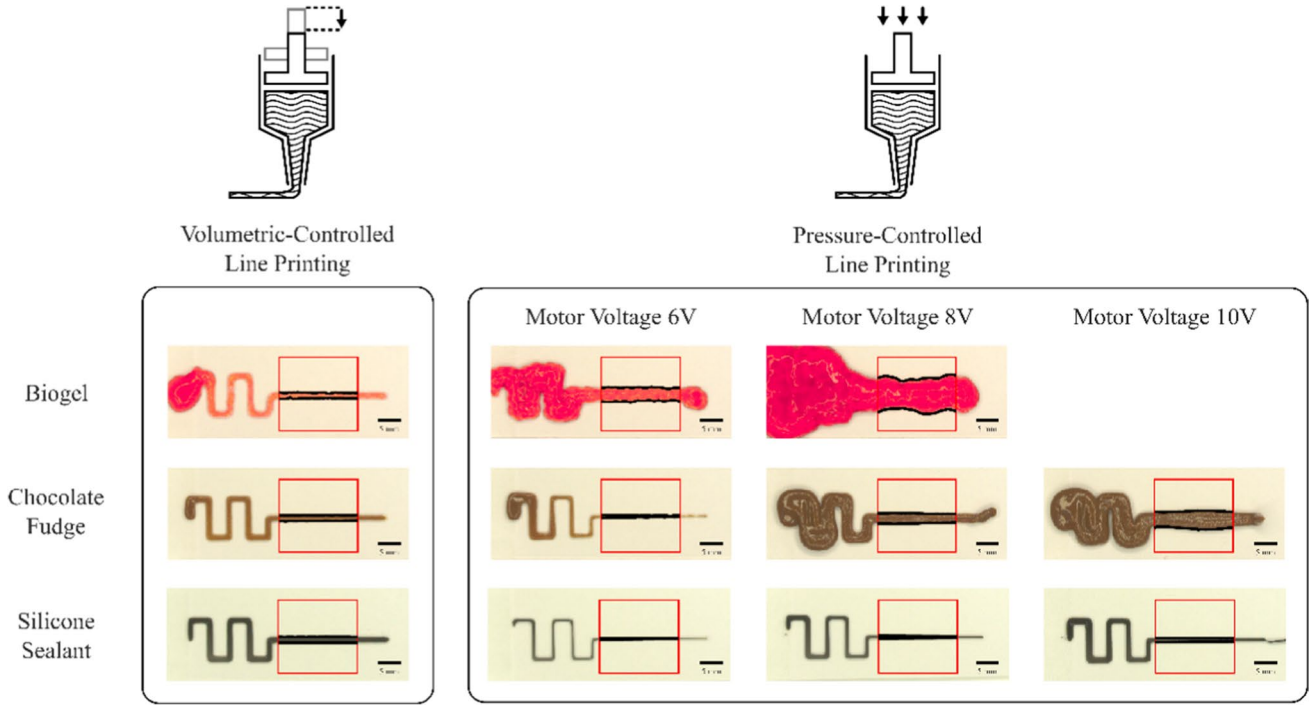

Fig. 7 The printed lines use volumetric-controlled and pressure-controlled extrusion. The selected regions are indicated by red squares. These are areas wherein both mean and standard deviation of line width are extracted. The black scale bars in the photos are 5 mm in length

Table 3 Mean line width (μ) in the unit of mm with standard deviations (σ)

Materials	Position controlled		Pressure controlled					
	μ	σ	Motor voltage 6 V		Motor voltage 8 V		Motor voltage 10 V	
			μ	σ	μ	σ	μ	σ
Biogel	1.4254	0.1080[1]	3.4999	0.1890	8.4479	0.6639	N/A	N/A
Chocolate fudge	1.5267	0.0394[1]	0.4972	0.1683	2.5965	0.1945	4.3951	0.3695
Silicone sealant	1.5531	0.0142[1]	0.2866	0.0347	0.6574	0.0665	0.9613	0.0725

[1]The lowest standard deviation value for each material

3.3 Intrinsic sensing: heterogeneous mixture extrusion

In this experiment, a non-homogeneous hydrogel mixture was extruded, using the proposed technique. During extrusion, machine vision was used to capture the flow. A video was synchronized with the signals from the ram extruder's microcontroller. Throughout the extrusion of the non-homogeneous hydrogel mixture, piston feed rate error and motor current were plotted over time (Fig. 8).

At the beginning of the extrusion, regular hydrogel flowed through the nozzle and escaped through the tip of the nozzle. Feed rate error stabilized around the value of 0 mm/s while the motor current increased slowly. After 1 s, a small part of the highly concentrated gel was forced through the narrow area at the lowest section of the syringe. Due to an increase in resistance, the same pressure applied could not maintain the constant flow of the material anymore. Consequently, both feed rate error and motor current sharply increased to around 1 mm/s and 1.2 A, respectively.

During the next 0.5-s period, a greater volume of the viscous gel was pushed through the bottleneck of the syringe, corresponding with the steadiness of the two variables at the raised values. At about 1.5 s, the concentrated gel detached from the main body and slipped into the broadest part of the nozzle (uppermost). When the resistance at the bottleneck sharply dropped, the internal stress of the material in the syringe lowered instantly. Thereupon, the residual gel in the nozzle squirted out. This overflow resulted in a drastic drop

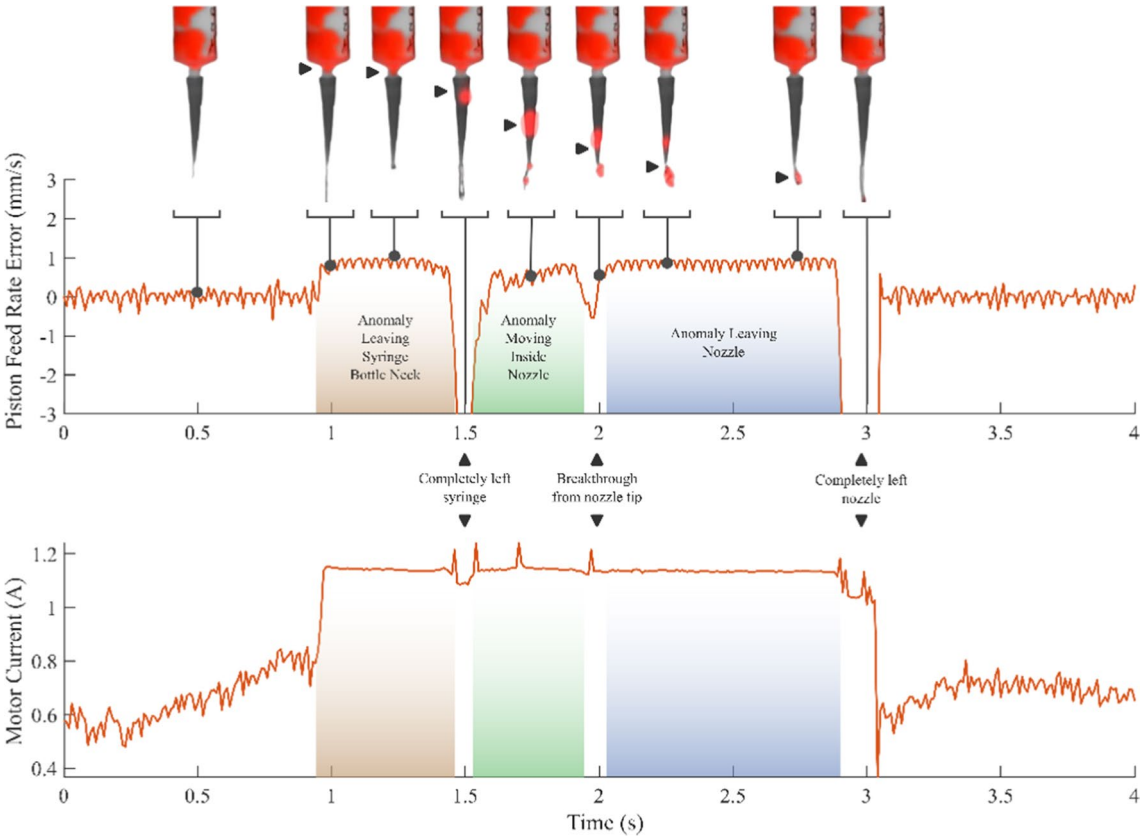

Fig. 8 Schema of intrinsic sensing: visibility of printing material. Anomaly infested material is represented by a non-homogeneous biogel formed by mixing concentrated biogel (red) in its regular counterpart (transparent). Piston feed rate error is calculated by the difference between the reference feed rate and the actual feed rate measured by the encoder. The trend of this parameter corresponds with the location of the anomaly, which is illustrated by black triangles. The motor current is measured by the motor driver chip and is proportional to the force that the motor exerts

in feed rate error and a slight drop in motor current. The detached gel in the nozzle then drifted down toward the tip. Thereby, more effort from the motor was required to push it through the smaller cross-sectional area. Hence, the feed rate error slowly increased while the motor current remained steady at an elevated level.

At roughly 2 s, part of the fragment began to escape through the nozzle tip. This process continued for almost 1 s, while both feed rate error and motor current were maintained at the ascended values. At around 2.9 s, the detached gel fully exited from the tip of the nozzle. The instant the pressure was released, the overflow of the material oozed out of the nozzle, bringing about a sharp drop in feed rate error along with a small drop in motor current. In the next 0.2 s approximately, a rapid decrease in the current took place. Feed rate error once again converged around the value of 0 mm/s, while the motor current dropped back and slightly fluctuated around 0.7 A.

As for the actual case of viscoelastic material, the flow is highly complex as the material possesses both properties of solid and fluid. The material needs to be compressed through the taper of the nozzle. In essence, the deformation and flow of matter are very difficult to model and are sensitive to disturbances such as temperature. It is also noted that even if the temperature is controlled, it is still challenging to guarantee that the temperature inside the syringe is uniform. This complication of rheology may reflect the pressure and flow.

In the demonstration, the proposed prototype can detect the difference in rheology as the material suddenly gains more viscosity and stiffness. In Fig. 8, results show the potential usage of the thresholding method to detect clogging inside the nozzle. In the graph, the piston feed rate error of 0.5 mm/s can be used to detect anomalies. Such a technique may further be used in real applications to prevent print failure.

Furthermore, the signal that is demonstrated reflects the flushing completion when the clog is flushed out (Fig. 8). The drastic drop in feed error is highly related to the breakthrough of the clog. Using the threshold technique, this event is easily detected. The proposed hardware has the potential to detect clogs in real time during the printing process and is also able to sense the completion of clog flushing.

3.4 Discussion

Greater repeatability of material extrusion can be achieved by controlling the initial conditions of the flow. Unlike pure elastic or pure viscous materials, viscoelasticity exhibits the exponential relaxation of stress over time. The difference in initial residual stress will affect the flow behavior of the material. Thus, starting the process from the same internal pressure is favorable. The experiment demonstrates that relatively higher-pressure stability can be attained by utilizing constant voltage driving. Arguably, the internal pressure from the volumetric-controlled flushing process might converge at some point. Yet, the time required for this to occur is seen to be significantly longer.

In contrast, line laying, using a pressure-based actuation approach, proved to be quite challenging. The characteristics of printed lines are profoundly affected by the viscosity and elasticity of the material. When stress is applied, the viscosity describes the deformation rate of the material. Viscosity dictates the amount of material extruded at a certain pressure, thus governing the mean width of the printed line. In the mass spring damper system, the higher spring constant results in a larger amplitude and frequency. Similarly, materials with higher elastic modulus can store more residual stress, resulting in higher deviation in the width.

The control of line width is hardly possible without intensive calibration of the print pressure on the material. Moreover, the change in the viscosity of the material caused by time, temperature change, and chemical reactions can influence the conditions of the printed line [27]. At steady state, higher resilience of material properties can be achieved by manipulation of the piston position rather than the internal pressure of the material. The volumetric-controlled extrusion method signifies greater reliability and superior uniformity of the line width.

In the last experiment, material sensing capability was demonstrated. The measured response suggests that the system can successfully distinguish between regular and highly viscous gel while it travels through the bottleneck of the syringe and out through the nozzle. This experiment indicates that the viscosity of the material can be sensed by the proposed hardware, as demonstrated in the simulation.

With proper calibration, the proposed design might be able to sense the properties of an unknown material stored in the syringe and adjust the printing profile, according to the material. The ability to detect and resolve unexpected anomalies might also be possible if the change in viscosity is present, e.g., (a) re-printing of the disconnected line caused by bubbles in the material and (b) mid-print flushing in the case where sediment in the nozzle is encountered.

4 Conclusion

Herein, a novel flexible actuation system with intrinsic sensing demonstrates its ability to sense pressure and flow rate from the actuator's side. Unlike conventional LDM actuation, our system can control the extrusion in both modes: pressure controlled and volumetric controlled. Overall, the system encompasses nonlinear dynamics, and the material displays viscoelastic behavior; control of pressure offers better handling of flow initialization. Volumetric control ensures more precise flow in steady state. In pressure control mode, volumetric flow is real-time sensible. Vice versa, in volumetric flow mode, pressure is real-time monitored. Only a limited number of studies have investigated the extruder's ability to intrinsically sense the properties of print material, which is considered in our work. With this design, the loaded material's properties, such as viscosity, can be revealed during actuation, providing useful insight into the extrusion process. This work lays a strong foundation for further development and optimization of the printhead, which is a critical part of LDM technology.

Author contribution SS contributed in data curation, investigation, methodology, hardware, validation, visualization, and writing of original draft. CS contributed in conceptualization, methodology, and project administration. KC contributed in data curation, formal analysis, methodology, software, validation, and visualization. RC contributed in conceptualization, funding acquisition, project administration, and supervision. All authors commented on previous versions of the manuscript. All authors read and approved the final manuscript.

Funding This project is funded by National Research Council of Thailand (NRCT).

Declarations

Conflict of interest The authors declare no competing interests.

References

1. Valino AD, Dizon JRC, Espera AH et al (2019) Advances in 3D printing of thermoplastic polymer composites and nanocomposites. Prog Polym Sci 98:101162. https://doi.org/10.1016/j.progpolymsci.2019.101162

2. Lewis JA (2006) Direct ink writing of 3D functional materials. Adv Funct Mater 16:2193–2204. https://doi.org/10.1002/adfm.200600434
3. Chen Q, Cao P, Advincula RC (2018) Mechanically robust, ultraelastic hierarchical foam with tunable properties via 3D printing. Adv Funct Mater 28:. https://doi.org/10.1002/adfm.201800631
4. Gratson GM, Xu M, Lewis JA (2004) Microperiodic structures: direct writing of three-dimensional webs. Nature 428:386–386. https://doi.org/10.1038/428386a
5. M'Barki A, Bocquet L, Stevenson A (2017) Linking rheology and printability for dense and strong ceramics by direct ink writing. Sci Rep 7:6017. https://doi.org/10.1038/s41598-017-06115-0
6. Kalita SJ, Bose S, Hosick HL, Bandyopadhyay A (2003) Development of controlled porosity polymer-ceramic composite scaffolds via fused deposition modeling. Mater Sci Eng, C 23:611–620. https://doi.org/10.1016/S0928-4931(03)00052-3
7. Hong S, Sanchez C, Du H, Kim N (2015) Fabrication of 3D printed metal structures by use of high-viscosity Cu paste and a screw extruder. J Electron Mater 44:836–841. https://doi.org/10.1007/s11664-014-3601-8
8. Jakus AE, Taylor SL, Geisendorfer NR et al (2015) Metallic architectures from 3D-printed powder-based liquid inks. Adv Funct Mater 25:6985–6995. https://doi.org/10.1002/adfm.201503921
9. Malda J, Visser J, Melchels FP et al (2013) 25th anniversary article: engineering hydrogels for biofabrication. Adv Mater 25:5011–5028. https://doi.org/10.1002/adma.201302042
10. Heo DN, Alioglu MA, Wu Y et al (2020) 3D bioprinting of carbohydrazide-modified gelatin into microparticle-suspended oxidized alginate for the fabrication of complex-shaped tissue constructs. ACS Appl Mater Interfaces 12:20295–20306. https://doi.org/10.1021/acsami.0c05096
11. de Oliveira RS, Funk NL, dos Santos J et al (2022) Bioadhesive 3D-printed skin drug delivery polymeric films: from the drug loading in mesoporous silica to the manufacturing process. Pharmaceutics 15:20. https://doi.org/10.3390/pharmaceutics15010020
12. Hossain SS, Son H-J, Park S, Bae C-J (2023) Extrusion-based 3D printing alumina-silica inks: adjusting rheology and sinterability incorporating waste derived nanoparticles. J Eur Ceram Soc 43:4865–4876. https://doi.org/10.1016/j.jeurceramsoc.2023.03.068
13. Rau DA, Bortner MJ, Williams CB (2023) A rheology roadmap for evaluating the printability of material extrusion inks. Addit Manuf 75:103745. https://doi.org/10.1016/j.addma.2023.103745
14. Rau DA, Williams CB, Bortner MJ (2023) Rheology and printability: a survey of critical relationships for direct ink write materials design. Prog Mater Sci 140:101188. https://doi.org/10.1016/j.pmatsci.2023.101188
15. Arif ZU, Khalid MY, Noroozi R et al (2023) Additive manufacturing of sustainable biomaterials for biomedical applications. Asian J Pharm Sci 18:100812. https://doi.org/10.1016/j.ajps.2023.100812
16. Kolesky DB, Truby RL, Gladman AS et al (2014) 3D Bioprinting of vascularized, heterogeneous cell-laden tissue constructs. Adv Mater 26:3124–3130. https://doi.org/10.1002/adma.201305506
17. Khalil S, Sun W (2007) Biopolymer deposition for freeform fabrication of hydrogel tissue constructs. Mater Sci Eng, C 27:469–478. https://doi.org/10.1016/j.msec.2006.05.023
18. Karis DG, Ono RJ, Zhang M et al (2017) Cross-linkable multistimuli responsive hydrogel inks for direct-write 3D printing. Polym Chem 8:4199–4206. https://doi.org/10.1039/C7PY00831G
19. Fedorovich NE, Swennen I, Girones J et al (2009) Evaluation of photocrosslinked lutrol hydrogel for tissue printing applications. Biomacromol 10:1689–1696. https://doi.org/10.1021/bm801463q
20. Mandrycky C, Wang Z, Kim K, Kim D-H (2016) 3D bioprinting for engineering complex tissues. Biotechnol Adv 34:422–434. https://doi.org/10.1016/j.biotechadv.2015.12.011
21. Kazmer DO, Kodra S, Mubasshir AA et al (2021) Additive ram material extrusion and diddling of fully compounded thermoset nitrile rubber. Polym Compos 42:5237–5248. https://doi.org/10.1002/pc.26218
22. Deuser BK, Tang L, Landers RG, et al (2013) Hybrid extrusion force-velocity control using freeze-form extrusion fabrication for functionally graded material parts. J Manuf Sci Eng 135:. https://doi.org/10.1115/1.4024534
23. Chaiprabha K (2023) An intrinsic sensing ram extruder with pressure and volumetric flow control for liquid deposition modeling. Chulalongkorn University
24. Vahid-Araghi O, Golnaraghi F (2011) Friction-induced vibration in lead screw drives. Springer, New York, New York, NY
25. Bacciotti A, Rosier L (2005) Liapunov functions and stability in control theory. Springer, Berlin Heidelberg, Berlin, Heidelberg
26. Kypuros J (2013) System dynamics and control with bond graph modeling. CRC Press
27. Li K, Zhao J, Zhussupbekova A et al (2022) 4D printing of MXene hydrogels for high-efficiency pseudocapacitive energy storage. Nat Commun 13:6884. https://doi.org/10.1038/s41467-022-34583-0